Published in final edited form as:
Biomaterials. 2010 August ; 31(24): 6182–6189. doi:10.1016/j.biomaterials.2010.04.041.

Effect of Mechanical Factors on the Function of Engineered Human Blood Microvessels in Microfluidic Collagen Gels

Gavrielle M. Price, **Keith H. K. Wong**, **James G. Truslow**, **Alexander D. Leung**, **Chitrangada Acharya**, and **Joe Tien***
Department of Biomedical Engineering, Boston University, 44 Cummington Street, Boston, MA 02215

Abstract

This work examines how mechanical signals affect the barrier function and stability of engineered human microvessels in microfluidic type I collagen gels. Constructs that were exposed to chronic low flow displayed high permeabilities to bovine serum albumin and 10 kDa dextran, numerous focal leaks, low size selectivity, and short lifespan of less than one week. Higher flows promoted barrier function and increased longevity; at the highest flows, the barrier function rivaled that observed in vivo, and all vessels survived to day 14. By studying the physiology of microvessels of different geometries, we established that shear stress and transmural pressure were the dominant mechanical signals that regulated barrier function and vascular stability, respectively. In microvessels that were exposed to high flow, elevation of intracellular cyclic AMP further increased the selectivity of the barrier and strongly suppressed cell proliferation. Computational models that incorporated stress dependence successfully predicted vascular phenotype. Our results indicate that the mechanical microenvironment plays a major role in the functionality and stability of engineered human microvessels in microfluidic collagen gels.

Keywords

Mechanical microenvironment; barrier function; microvascular tissue engineering; shear stress; transmural pressure

1. Introduction

Early studies of transplanted tissues have established that most millimeter-sized grafts require perfusion with blood within 3–4 days to survive [1–4]. Inosculation between microvessels of the host and those in the implanted tissue led to timely reperfusion of the graft; in-growth of host vessels also contributed to viability of a graft, depending on the source of tissue. Given the central importance of rapid establishment of perfusion in obtaining a viable graft, we and others have attempted to engineer “pre-vascularized” constructs that could potentially accelerate (re)perfusion upon transplantation [5–8]. Strategies for pre-vascularization span a wide range, from the incorporation of individual endothelial cells [5,6] to the use of microvascular fragments [8] or even entire vascular loops [7].

Corresponding author: Telephone: 617-358-3055, Fax: 617-353-6766, jtien@bu.edu.

While providing perfusion is a critical function of engineered microvessels, it is not the only one. In vivo, blood vessels serve many physiological functions besides serving as open tubes, including prevention of thrombosis [9], modulation of solute efflux [10], regulation of diapedesis [11], autoregulation of blood flow [12], secretion of cytokines [13], and presentation of antigens [14]. For engineering tissues that are intended to have continuous vessels (e.g., dermis, adipose, and muscle), barrier function and long-term vascular stability are likely to be required. In these tissues, sustained breakdown of the vascular barrier can lead to edema, which results in inappropriate interstitial forces and flows that compromise the health of surrounding parenchyma [15].

Recently, we have developed methods to form and vascularize microfluidic channels within gels of extracellular matrix [16–19]. These channels, and the vessels that form from them, can be perfused immediately and continuously. We view this work as a step toward designing custom-made vascular beds that can sustain the metabolic requirements of a tissue construct and that can eventually be integrated into the vascular system of a host. These short-term studies have focused largely on obtaining open endothelial tubes or networks that resemble the topology of normal microvascular beds. To what extent the immature vascular structures can remain patent and/or exhibit vascular functions is largely unknown.

Here, we examine how mechanical signals affect the phenotype of engineered human microvessels in microfluidic type I collagen gels. Previous work by numerous groups has shown that mechanical signals, such as hydrostatic pressure, stretch, and shear stress, exert pleiotropic effects on vascular function [20–24]. Acute increases in shear stress weakened the barrier of microvessels in vivo and endothelial monolayers in vitro [25–27]; chronic exposure (≥24 hrs) to elevated shear appeared to enhance barrier function in vitro [28]. Exposure to increased transmural pressure across the endothelium transiently enhanced the barrier in vivo and in vitro (the so-called “sealing effect”), followed by weakening of barrier [29–31].

The purpose of our study was to determine how chronic exposure to various mechanical factors affected the barrier function and stability of engineered microvessels. We maintained vessels under different flow conditions to quantify the effects of flow rate, shear stress, transmural pressure, and average lumenal pressure on vascular phenotype. We used three vascular configurations in these experiments: 1) single (nearly) cylindrical tubes, in which all four mechanical factors varied in unison, 2) tubes that had sharply tapered profiles, which selectively allowed large intravascular variations in shear stress, and 3) tubes that were adjacent to empty channels, which selectively reduced transmural pressure. Using these configurations, we determined the mechanical signals that were the dominant regulators of barrier function and stability. We used computational models that incorporated a mechanically sensitive phenotype to better understand the forces and flows within these constructs. Moreover, since we recently showed that elevation of intracellular cyclic AMP (cAMP) partially normalized the function of engineered vessels [32], we studied whether the co-presence of cAMP-elevating agents and mechanical factors led to synergistic improvements in vascular phenotype.

2. Materials and methods

2.1. Cell culture

Endothelial cells from human dermal blood microvessels (BECs; lots 5F1293 and 6F4144 from Lonza, and lot 7082905.1 from Promocell) were grown on gelatin-coated dishes in MCDB 131 media (Caisson Labs) with 10% heat-inactivated FBS (Atlanta Biologicals), 1% glutamine-penicillin- streptomycin (Invitrogen), 80 μM dibutyryl cAMP (db-cAMP; Sigma), 1 μg/mL hydrocortisone (Sigma), 2 U/mL heparin (Sigma), 25 μg/mL endothelial cell growth supplement (Biomedical Technologies), and 0.2 mM ascorbic acid 2-phosphate (Sigma).

Cultures were routinely passaged using dispase (2 U/mL in PBS) at a 1:4 ratio onto gelatin-coated tissue culture plates. Cells were discarded after passage 7.

2.2. Formation and vascularization of microfluidic collagen gels

Tubes of BECs (n = 178) were formed by modification of previously described methods [16, 33]. To form (nearly) cylindrical microvessels, we gelled type I collagen (final concentration of 7–8 mg/mL from rat tail; BD Biosciences) around 120-μm-diameter stainless steel needles (Seirin). Careful removal of needles yielded open-ended, ~9-mm-long cylindrical channels in gels. Confluent cultures of BECs were trypsinized and seeded as a suspension into the bare channels via wells at the inlet and outlet. Cells spread and grew to confluence to form open tubes by day 2 post-seeding.

To form tapered microvessels, we etched 120-μm-diameter needles by sonicating them in nickel etchant (Transene Corporation) at 23°C for 5–8 min [16]. The etched portions were 60–80 μm in diameter. Needles were washed thoroughly with deionized H_2O and used as described above to form tapered tubes of BECs within collagen gels.

To form parallel pairs of BEC tubes and bare channels, we gelled collagen around two 120-μm-diameter needles placed side-by-side. One needle was removed, and the resulting channel was seeded as described above. After seeding, the inlet and outlet ends of the gel were thoroughly washed with media to remove unattached cells. The second needle was then withdrawn to yield a bare channel in parallel with the seeded one. The seeded and unseeded channels shared the same inlet and outlet.

2.3. Perfusion of microvessels

All microvessels were perfused with culture media supplemented with 3% 70 kDa dextran (Sigma) via wells at the inlet and outlet. In some cases, the perfusate was supplemented with 400 μM db-cAMP and 20 μM of the phosphodiesterase inhibitor Ro-20-1724 (Calbiochem) [33,34]. The viscosity of perfusate was calculated by comparing the flow rate of perfusate to that of H_2O at 37°C in ~50-cm-long segments of tubing.

Perfusion was established by connecting the inlet and outlet wells of microvessels to dishes of media that were held at different heights. All tubing was calibrated to a fluidic resistance of 0.46 cm H_2O·hr/mL. Media was recycled 1–2 times per day, and replaced every 2–3 days.

For cylindrical and tapered microvessels, we calculated local shear stress as $\tau = \frac{4Q\eta}{\pi r^3}$ and average lumenal pressure as $P_{avg} = \frac{P_{in} + P_{out}}{2}$. Here, Q is the flow rate, η is the viscosity of perfusate, r is the local vascular radius, and P_{in} and P_{out} are the inlet and outlet pressures of the microvessel (corrected for pressure losses within tubing).

To determine the shear stress in a vessel that is parallel with a bare channel, we first calculated the flow rate through the bare channel as $Q_{bare} = \frac{(P_{in} - P_{out}) \cdot \pi r_{bare}^4}{8\eta L}$, where L is the length of the channel and r_{bare} = 60 μm is the radius. We then used the difference between the measured flow rate Q and calculated Q_{bare} to find shear stress as $\tau = \frac{4(Q - Q_{bare})\eta}{\pi r^3}$.

2.4. Measurement of permeabilities

All permeability measurements took place on day 3 post-seeding, largely as described previously [35,36]. Alexa Fluor 594-conjugated bovine serum albumin (BSA) (50 μg/mL;

Invitrogen) and Alexa Fluor 488-conjugated 10 kDa dextran (20 μg/mL; Invitrogen) were introduced into the microvessel by perfusion. Fluorescence images were then taken once every minute until at least 10 minutes after the flow of fluorescent solutes within the lumen became fully developed. Imaging took place in an environmental chamber held at 37°C. All images were obtained through a Plan-Neo 10×/0.30 NA objective, and were corrected for intensity variations across the field-of-view with Axiovision 4.3 (Zeiss). Effective permeability coefficients P_e were calculated from the equation $P_e = \frac{1}{\Delta I} \cdot \frac{dI}{dt} \cdot \frac{r}{2}$, where ΔI is the initial increase in fluorescence intensity from background intensity, and dI/dt is the rate of increase in fluorescence intensity after flow was fully developed.

Focal leaks (i.e., visibly leaky sites along the vessel wall) were counted manually after maximizing image contrast, and are given as the number of leaks per frame per surface area of endothelium, approximating vessel geometries as cylinders.

2.5. Immunostaining and quantification of junctions

On day 3 post-seeding, microvessels were fixed by perfusion with 4% paraformaldehyde (PF) for 20 min, and then permeabilized and blocked in 5% goat serum (GS), 0.2% Triton X-100 (TX-100), and 10 mM glycine for 1 hr. Microvessels were then perfused with mouse anti-PECAM-1 (1:200, clone WM-59; Sigma) or mouse anti-VE-cadherin (1:100, clone 75; BD Transduction Laboratories) for 1 hr, incubated overnight at 4°C, flushed by perfusion with 5% GS, 0.1% TX-100, and 10 mM glycine for 1 hr at 22°C, perfused with Alexa Fluor 488-conjugated goat anti-mouse secondary antibody (1:500; Invitrogen) for 1 hr at 22°C, and then exhaustively flushed. Nuclei were visualized with Hoechst 33342 (1 μg/mL) for 10 min. Confocal images were taken through a Plan-Apo 10×/0.40 NA objective using an Olympus IX81 inverted microscope. Sequential images from the bottom to mid-plane of each microvessel were taken at 4.3 μm spacing and stacked with ImageJ 1.38 (NIH).

Junctional staining for VE-cadherin was quantified by measuring the average lengths of uninterrupted VE-cadherin staining, as described previously [33].

2.6. Measurement of leak area

To irreversibly label leaks in tapered or parallel tubes, we tagged an antibody to type I collagen (clone COL-1; Sigma) with Alexa Fluor 488-conjugated Fab fragments according to the supplier's protocol (Zenon; Invitrogen) and then perfused microvessels with 1 μg/mL of the labeled antibody (~2 μg/mL of the antibody-Fab complex) for ≥1 hr, as described recently [32]. Microvessels were then flushed of soluble antibody for ≥1 hr and fixed by perfusion with 4% PF for 20 min. Confocal images were obtained as described above.

All pixels above a background intensity threshold were identified using a MATLAB script. Fractional leak area was expressed as the ratio of labeled pixels to total pixels.

2.7. Determination of vascular lifespan

Cylindrical microvessels were perfused under different flow conditions until day 14 post-seeding or until the microvessels became unstable. Microvessels were considered unstable ("dead" in Kaplan-Meier analysis) if the endothelium had delaminated from the collagen gel and/or if the flow rate decreased by 50%. Delamination near vessel outlets did not interfere with viability and was not noted.

2.8. Quantification of morphological stability

The extent of delamination was calculated as the total length of exposed collagen per length of microvessel, with a maximum value of one corresponding to complete delamination. Sprout

density was calculated as the total number of invasive structures per length of microvessel. We only counted sprouts that were directly connected to the vessel wall.

2.9. Proliferation assay

On day 3 post-seeding, microvessels were perfused with 10 μM 5-ethynyl-2′-deoxyuridine (EdU; Invitrogen) for ≥4 hr. Microvessels were flushed with EdU-free perfusate, fixed by perfusion with 4% PF for 20 min, and permeabilized with 5% GS, 0.2% TX-100, and 10 mM glycine for 1 hr at 22°C. EdU was detected by click chemistry with Alexa Fluor 594 azide according to the supplier's protocol; nuclei were visualized with Hoechst 33342.

2.10. Computational modeling

Stress and strain for the three experimental configurations were calculated using finite-element models (COMSOL Multiphysics 3.5a). Each model was solved using an iterative procedure: First, the Navier-Stokes equations were solved to obtain lumenal velocities and pressures; we assumed that vascular filtration rate was negligible in comparison to lumenal flow. Second, Darcy's Law was solved to obtain pressures within the gel, using the small filtration velocity from Starling's Law as a boundary condition. Third, the resulting transmural pressures were used to determine the radial strain of the vascular wall, assuming linearly elastic deformation of the gel. We repeated this sequence with the distended vascular profiles until the maximum difference in transmural pressures between iterations was ≤0.05 cm H_2O. We used the same tolerance to show mesh independence of each solution; the number of degrees-of-freedom was 100,000–200,000 for cylindrical and tapered tube models and ~700,000 for parallel tube models.

These models assumed a constant ratio between permeability to BSA (which we could measure) and endothelial hydraulic conductivity (which we could not measure) [10]. We set this ratio to be 500, 1000, or 2000 dyn/cm^2. Values for the other parameters were taken from previous studies [32,37].

2.11. Statistical analysis

Statistical analysis was performed with Prism 5 (GraphPad). Trends were analyzed by Spearman's rank correlation. Comparisons of grouped data used the Kruskal-Wallis test, followed by Mann-Whitney *U* test with Bonferroni correction for pairwise comparisons. Comparisons of survival curves used the log-rank test. Data are presented as arithmetic means ± 95% CI.

3. Results

3.1. Effect of flow on barrier function of engineered microvessels

At day 3 post-seeding, microvessels that were chronically exposed to low flow (Q ~ 0.5 mL/hr in ~120-μm-diameter tubes) were visibly permeable to the passage of fluorescent BSA or 10 kDa dextran across the endothelial wall; higher flows noticeably tightened the barrier (Fig. 1A). Increases in flow rate (0.07–4.4 mL/hr) were driven by increases in axial pressure difference (1.6–10.7 cm H_2O), and were accompanied by increases in shear stress (1.7–32.8 dyn/cm^2) and average lumenal pressure (0.95–7 cm H_2O). Higher flows also led to increased vascular diameter or radial strain (Fig. 1A), which most likely resulted from increased transmural pressure across the endothelial wall. As flow and its associated factors increased, the permeability coefficients to BSA (P_{BSA}) and 10 kDa dextran (P_{dex}) decreased, the number of focal leaks decreased to zero, and the size selectivity of the barrier—defined as P_{dex}/P_{BSA}—increased ($p < 0.0001$ for all trends; Fig. 1B). That is, flow improved barrier function.

Increased flow appeared to have an especially potent effect on focal leaks. Flow rates above ~1 mL/hr essentially eliminated leaks of this type. To understand the structural origin of this effect, we stained the vessels for VE-cadherin (a marker of endothelial adherens junctions that is associated with barrier function in vivo and in vitro [38,39]) and the endothelial marker PECAM-1. Vessels that were grown under low flow ($Q = 0.37 \pm 0.05$ mL/hr) displayed short, non-uniform expression of VE-cadherin at cellular junctions; segments of staining averaged 18.8 ± 0.7 μm in length. In contrast, vessels that were grown under high flow ($Q = 2.6 \pm 0.6$ mL/hr) displayed linear staining for VE-cadherin with much longer segments that averaged 31.5 ± 1.5 μm in length ($p < 0.0001$; Fig. 1C). We did not notice any differences in staining for PECAM-1. Thus, our data suggest that flow may have improved barrier function partly via enhanced junctional organization.

3.2. Effect of flow on vascular lifespan

Increased flow also significantly enhanced the lifespan of engineered vessels (Fig. 1D). Vessels were considered "dead" when the endothelium began to detach from the collagen wall and/or when the flow rate dropped to 50% of the maximum. At low flow ($Q = 0.56 \pm 0.04$ mL/hr), only one of fifteen vessels survived to day 14. When microvessels were maintained with medium ($Q = 1.4 \pm 0.1$ mL/hr) or high flow ($Q = 4.5 \pm 0.6$ mL/hr), nearly all vessels survived to at least day 14 ($p < 0.0001$ for medium or high flow compared to low flow).

3.3. Effect of lumenal pressure on barrier function

To determine whether a change in average lumenal pressure P_{avg} could alter barrier function by itself, we raised or lowered the dishes of media that drove perfusion, while holding their height difference constant. Using this method, P_{avg} varied from 1.0 to 6.9 cm H_2O, while flow rate (0.98 ± 0.05 mL/hr), axial pressure difference (4.5 ± 0.1 cm H_2O), shear stress (12.6 ± 0.6 dyn/cm^2), and strain (0.20 ± 0.02) remained relatively constant. We found that P_{avg} had little effect on permeability coefficients, size selectivity, and focal leaks: In each case, the linear regression of the data did not significantly differ from a slope of zero ($p > 0.1$; Fig. 2A).

3.4. Effect of shear stress and radial strain on morphological stability

To distinguish the effects of shear stress and radial strain on vascular phenotype, we formed vessels in two new configurations: tapered vessels (Fig. 2B) and vessels that were parallel with bare channels (Fig. 2C). In tapered microvessels, the upstream segments were wider than the downstream ones. Since the same flow passed through both segments, much lower shears existed upstream than downstream. By day 3 post-seeding, shear stresses in the upstream and downstream segments were 5.1 ± 1.2 dyn/cm^2 and 23.3 ± 3.4 dyn/cm^2, respectively; the range of driving pressure differences was 7.5–12.8 cm H_2O. Notably, both segments distended similarly (strains of 0.62 ± 0.09 upstream and 0.57 ± 0.10 downstream).

In vessels that were parallel with bare channels, we expected the presence of the bare channel to increase pressure within the surrounding gel and thus minimize strain in the neighboring vessel (Fig. 2C). These microvessels were maintained either with low or high shear. Vessels exposed to high shear (24.2 ± 2.8 dyn/cm^2) had small radial strains (0.04 ± 0.05). Vessels exposed to low shear invariably displayed widespread delamination by day 3 post-seeding (Fig. 2C, top panel). While microvessels that were placed in the parallel geometry and exposed to high shear did not delaminate or collapse, this setup resulted in invasion of endothelial cells into the surrounding collagen, visualized as sprouts along the vessel wall (Fig. 2C, bottom panel).

These data suggest that positive strain (i.e., a positive transmural pressure) is required to obtain morphologically stable vessels, irrespective of the level of shear stress. In tapered microvessels, which exhibited positive strain, no or few (0.4 ± 0.4 per mm) sprouts emerged along the low-

or high-shear regions, respectively (Fig. 2D). In parallel microvessels, which exhibited nearly zero strain, the density of sprouts was 1.8 ± 1.4 per mm and 8.1 ± 4.1 per mm under low and high shear, respectively ($p = 0.009$ and <0.0001, compared to high-shear regions of tapered vessels). Only in parallel vessels maintained under low shear did delamination occur; the ratio of total length of delaminating regions to the length of the microvessel was 0.42 ± 0.14 (Fig. 2E).

3.5. Effect of shear stress and radial strain on barrier function

We used the same two configurations (tapered tube, parallel tube and channel) to determine the relative roles of shear and strain on barrier phenotype. Here, fluorescently-labeled antibodies to type I collagen were used to irreversibly label sites of leakage along the endothelium, since the standard permeability assay with BSA or dextran could not be applied. Labeling was quantified as the area of positive signal per area of endothelium. Upstream segments of tapered microvessels displayed noticeably more leaks than the downstream regions did (Fig. 2B). Moreover, parallel vessels under high shear had few leaks, while those under low shear were too leaky to be assayed. Overall, leak area was significantly anti-correlated with shear stress ($p < 0.0001$; Fig. 2F). No correlation existed between leak area and strain ($p > 0.05$; Fig. 2G). Immunostaining of tapered microvessels for VE-cadherin revealed that low-shear regions had disorganized junctions, while high-shear regions displayed continuous expression of VE-cadherin (Fig. 2B). Taken together, these results indicate that shear stress was the dominant regulator of microvessel barrier, whereas strain (and, thus, transmural pressure) had little effect.

3.6. Computational modeling of vascular phenotype

To better understand the forces and flows present in vascularized scaffolds, we used computational models to predict the shear stress and gel and lumenal pressures in five situations: 1) a cylindrical tube under high flow, 2) a cylindrical tube under low flow, 3) a tapered tube, 4) a parallel tube and channel under high flow, and 5) a parallel tube and channel under low flow (Fig. 3). These models assumed that barrier function was a function of shear stress only (using the linear fit in Fig. 1B), and that stability required positive transmural pressure. Any major discrepancy between the prediction of these models and experimental results would thus indicate that the effects of shear stress and transmural pressure were insufficient to account for the effects of flow.

Remarkably, these somewhat simplistic models corroborated essentially all of our experimental findings. For the cylindrical and tapered cases, the models indicated that gel pressures were nearly equal to the pressure at the outlet. The reason for this finding is that the low shear and initially negative transmural pressure along the outer surface of the collagen gel adjacent to the outlet led to a leaky and unstable endothelium there. The resulting lack of any functional barrier between the gel and outlet resulted in near-equilibration of pressures in the two compartments. Although a low shear also exists along the surface of the gel adjacent to the inlet, here transmural pressure is positive, the endothelium is predicted to be stable (albeit leaky), and the gel is partly insulated from the pressure at the inlet. Because the gel pressure is nearly equal to the outlet pressure, the transmural pressure along the vessel wall is positive. Models of cylindrical tubes predicted that high flow rates would lead to high transmural pressures and radial strains, as was observed experimentally. Moreover, a slight tapering of the vascular wall profile (widest at the inlet, less widened at the outlet) was predicted, also in agreement with experiment and as observed previously [16].

As intended, the presence of the bare channel in the parallel setup equilibrated gel and lumenal pressures; as a result, the computed transmural pressure was nearly zero along the vessel wall in these cases.

Our computational results indicated that the local barrier and stability phenotypes obtained experimentally, when applied globally to the entire surface of a vessel, can predict the shape and phenotype of that vessel. The consistency between prediction and experiment provides further evidence that shear stress and transmural pressure are the primary determinants of flow-mediated effects in our constructs.

3.7. Effect of cyclic AMP-elevating agents on vessels grown under high flow

Recently, we established that elevation of intracellular cyclic AMP (cAMP) led to partial normalization of vascular function in microfluidic collagen gels [32]. Specifically, cAMP-elevating agents enhanced barrier function, increased lifespan, and decreased cell turnover. Given the overlap in effects by cAMP and flow, we determined whether the co-presence of high cAMP levels and high flow would lead to further enhancement of vascular function.

Microvessels under high flow ($Q = 2.5 \pm 0.1$ mL/hr) were treated with 80 μM db-cAMP (the standard concentration in perfusate) or 400 μM db-cAMP and 20 μM Ro-20-1724, a phosphodiesterase inhibitor that augments the intracellular concentration of cAMP [34]. We found that high concentrations of cAMP did not cause any significant change in permeability coefficients ($p > 0.2$; Fig. 4A-B), but did lead to a slight increase in selectivity of the barrier ($p = 0.03$; Fig. 4C). As expected, we did not observe any focal leaks in microvessels under either condition. Consistent with previous work, high levels of cAMP drastically reduced proliferation in microvessels ($p < 0.0001$; Fig. 4D), to levels observed in vivo. We did not measure the lifespan of these tubes, since we found that high levels of cAMP already increased survival to at least two weeks [32]. These data indicated that high levels of cAMP and high flow together resulted in vessels that exhibited strong barrier function and low mitotic rates.

4. Discussion

4.1. Summary of findings

Barrier function and long-term vascular stability are required for proper perfusion of engineered tissues. Here, using tubes of human BECs in microfluidic type I collagen gels, we investigated the effect of mechanical signals on these desired outputs. Changes in flow rate altered three mechanical factors in concert: shear stress, lumenal pressure, and transmural pressure (as measured by radial strain). Increases in flow rate caused the endothelial barrier to tighten and increased vascular lifespan. These changes in permeability reflected changes in the organization of cell-cell junctions: The adherens junction marker VE-cadherin displayed more continuous staining as flow increased.

We found that changes in lumenal pressure could not account for flow-mediated effects. Rather, shear stress and transmural pressure played complementary roles in altering vascular phenotype. Shear stress was the dominant regulator of barrier function, while radial strain had little to no effect; stains for VE-cadherin supported this conclusion. Positive strain correlated with vascular stability, and inhibited endothelial delamination and/or invasion into the collagen gel.

These effects were complemented by those from cAMP-elevating agents. With high levels of shear, strain, and cAMP, vessels exhibited a tight, stable, and quiescent phenotype that rivaled the properties of mammalian microvessels in vivo. We note that the permeabilities obtained ($\sim 2\times10^{-7}$ cm/s for BSA) are well within the range found in vivo [40].

4.2. Mechanisms of flow-mediated changes

How do mechanical forces exert their local effects on vascular function? Regarding stability, it has long been thought that a minimum transmural pressure is necessary to prevent vessel

collapse in vivo [41]. Transmural pressure may stabilize the microvessel by physically compressing the endothelium against the collagen wall, thereby altering force balance. We found this physical explanation to account for stabilization induced by cAMP [32], and believe that it can also explain the findings of the current study. Biochemical signaling downstream of increased transmural pressure may also play a role in stabilization, although it is unclear how.

The barrier-promoting effects of shear stress, on the other hand, are almost certainly biochemical rather than physical in origin. While it is possible that added shear somehow mechanically distorts or compresses neighboring cells so as to narrow junctions or increase cell-cell overlap, previous work has shown that shear activates the small GTPase Rac, which leads to active reorganization of actin filaments [42]. In vivo, activation of Rac (via other mechanisms) enhances barrier function by increasing junctional area [43]. Surprisingly, acute change in flow leads to weaker barrier function in vivo, primarily through shear-mediated release of nitric oxide [25]. The discordant effects of increased shear in vivo and in vitro suggest that nitric oxide release is largely absent in our tubes; this explanation is consistent with the reported lack of glycocalyx in vitro, a structure that is required for shear stress-induced release of nitric oxide [44,45].

It is interesting to note that the co-presence of high shear stress and nearly zero strain did not lead to vascular collapse. Instead, the endothelium sprouted extensively into the surrounding gel, consistent with shear-mediated activation of Rac. Our results are consistent with those obtained by applying shear stress to endothelium on flat collagen gels, as the transmural pressure in these systems is likely close to zero [46,47]. We suspect that the sprouts act to "anchor" the vessel wall in the gel, thereby inhibiting collapse even though a stabilizing transmural pressure is absent.

In this analysis, we have treated radial strain as an indirect measure of transmural pressure. This assumption holds if endothelial contractility plays a negligible role in distension of the tube. In previous work [32], we found that contractility accounted for at most ~5% radial strain. Given that the strains in the current work typically exceeded this threshold (especially for high flow rates), changes in transmural pressure should account for much of the observed variation in strain between tubes.

4.3. Implications for vascularization of microfluidic scaffolds

Our results imply that a high shear stress and high transmural pressure must exist at all points along a vessel to obtain a tight and stable phenotype. How might these local conditions be established in a microfluidic scaffold? Establishment of high shear within a single channel is straightforward; one can always increase the driving pressure difference to obtain a desired level of shear. For scaffolds that contain interconnected vessels (i.e., a network), we expect that network geometries that favor the constancy of shear (i.e., with junctions that obey Murray's Law [48]) will be best suited for obtaining tight barrier function throughout the network. At minimum, shear stress should globally be held above 15–20 dyn/cm^2 to eliminate focal leaks (Fig. 1B).

How to establish high transmural pressure is not as obvious. From computational modeling, we found that the barrier phenotype at a distant point can influence local scaffold and transmural pressures. For dilute collagen gels (and other hydraulically conductive gels), the boundary conditions on the outer surface of the scaffold play an important role in determining local stresses within vascularized channels. For instance, the endothelium that covers the outlet end of our collagen gels existed under low shear and (initially) negative transmural pressure; these local conditions will result in a leaky, unstable phenotype that brings the scaffold pressures closer to the outlet pressure. Whether the transmural pressure along a vessel wall can remain positive everywhere will thus depend on how leaky the endothelium at the outlet is and,

conversely, on how tight the endothelium at the inlet is. For dense, resistive gels, it is likely that drainage channels will need to be built into a scaffold so that transmural pressure can be held positive, as we predicted in a recent study [37].

5. Conclusions

This work reports the effect of the mechanical microenvironment on the barrier properties and stability of engineered microvessels in microfluidic collagen gels. We found that increased flow led to stronger barrier function and greater stability via increases in shear stress and radial strain (or transmural pressure), respectively. These findings provide a set of guidelines—shear stress greater than 15–20 dyn/cm^2 and positive transmural pressure—for obtaining functional vascularization of collagen gels. We have only considered microfluidic gels in this work, and whether the design guidelines apply to other forms of vascularization (e.g., vessels that form by angiogenesis) remains to be determined.

Acknowledgments

We thank Celeste Nelson and Ken Chrobak for interesting discussions, Lee Lichtenstein for help with MATLAB, and Phil Allen for help with confocal imaging. This work was supported by the National Institute of Biomedical Imaging and Bioengineering (award EB005792) and by the National Heart, Lung, and Blood Institute (award HL092335). Part of this work was performed during sabbatical leave (J.T.) in the Nelson Group of the Department of Chemical Engineering at Princeton University.

References

1. Peer LA, Walker JC. The behavior of autogenous human tissue grafts. II Plast Reconstr Surg 1951;7:73–84.
2. Williams RG. The fate of minute blood vessels in omentum transplanted as autografts to the rabbit's ear. Anat Rec 1953;116:495–505. [PubMed: 13080691]
3. Merwin RM, Algire GH. The role of graft and host vessels in the vascularization of grafts of normal and neoplastic tissue. J Natl Cancer Inst 1956;17:23–33. [PubMed: 13346338]
4. Ausprunk DH, Knighton DR, Folkman J. Vascularization of normal and neoplastic tissues grafted to the chick chorioallantois. Role of host and preexisting graft blood vessels. Am J Pathol 1975;79:597–628. [PubMed: 1094838]
5. Schechner JS, Nath AK, Zheng L, Kluger MS, Hughes CC, Sierra-Honigmann MR, et al. *In vivo* formation of complex microvessels lined by human endothelial cells in an immunodeficient mouse. Proc Natl Acad Sci USA 2000;97:9191–6. [PubMed: 10890921]
6. Tremblay P-L, Hudon V, Berthod F, Germain L, Auger FA. Inosculation of tissue-engineered capillaries with the host's vasculature in a reconstructed skin transplanted on mice. Am J Transplant 2005;5:1002–10. [PubMed: 15816880]
7. Lokmic Z, Stillaert F, Morrison WA, Thompson EW, Mitchell GM. An arteriovenous loop in a protected space generates a permanent, highly vascular, tissue-engineered construct. FASEB J 2007;21:511–22. [PubMed: 17172640]
8. Shepherd BR, Chen HY, Smith CM, Gruionu G, Williams SK, Hoying JB. Rapid perfusion and network remodeling in a microvascular construct after implantation. Arterioscler Thromb Vasc Biol 2004;24:898–904. [PubMed: 14988090]
9. Rumbaut RE, Slaff DW, Burns AR. Microvascular thrombosis models in venules and arterioles *in vivo*. Microcirculation 2005;12:259–74. [PubMed: 15814435]
10. Michel CC, Curry FE. Microvascular permeability. Physiol Rev 1999;79:703–61. [PubMed: 10390517]
11. Ley K. The role of selectins in inflammation and disease. Trends Mol Med 2003;9:263–8. [PubMed: 12829015]
12. Duling BR, Klitzman B. Local control of microvascular function: role in tissue oxygen supply. Annu Rev Physiol 1980;42:373–82. [PubMed: 6996587]

13. Shepro, D.; D'Amore, P. Physiology and biochemistry of the vascular wall endothelium. In: Renkin, EM.; Michel, CC., editors. Handbook of Physiology; Section 2: The Cardiovascular System. Bethesda, MD: American Physiological Society; 1984. p. 103-64.
14. Pober JS, Gimbrone MA Jr, Lapierre LA, Mendrick DL, Fiers W, Rothlein R, et al. Overlapping patterns of activation of human endothelial cells by interleukin 1, tumor necrosis factor, and immune interferon. J Immunol 1986;137:1893–6. [PubMed: 3091693]
15. Swartz MA, Fleury ME. Interstitial flow and its effects in soft tissues. Annu Rev Biomed Eng 2007;9:229–56. [PubMed: 17459001]
16. Chrobak KM, Potter DR, Tien J. Formation of perfused, functional microvascular tubes in vitro. Microvasc Res 2006;71:185–96. [PubMed: 16600313]
17. Golden AP, Tien J. Fabrication of microfluidic hydrogels using molded gelatin as a sacrificial element. Lab Chip 2007;7:720–5. [PubMed: 17538713]
18. Price GM, Chu KK, Truslow JG, Tang-Schomer MD, Golden AP, Mertz J, et al. Bonding of macromolecular hydrogels using perturbants. J Am Chem Soc 2008;130:6664–5. [PubMed: 18454530]
19. Price, GM.; Tien, J. Subtractive methods for forming microfluidic gels of extracellular matrix proteins. In: Bhatia, SN.; Nahmias, Y., editors. Microdevices in Biology and Engineering. Boston, MA: Artech House; 2009. p. 235-48.
20. Davies PF. Flow-mediated endothelial mechanotransduction. Physiol Rev 1995;75:519–60. [PubMed: 7624393]
21. Tarbell JM, Demaio L, Zaw MM. Effect of pressure on hydraulic conductivity of endothelial monolayers: role of endothelial cleft shear stress. J Appl Physiol 1999;87:261–8. [PubMed: 10409584]
22. Schwartz EA, Bizios R, Medow MS, Gerritsen ME. Exposure of human vascular endothelial cells to sustained hydrostatic pressure stimulates proliferation. Involvement of the α_V integrins. Circ Res 1999;84:315–22. [PubMed: 10024305]
23. Nelson CM, Chen CS. VE-cadherin simultaneously stimulates and inhibits cell proliferation by altering cytoskeletal structure and tension. J Cell Sci 2003;116:3571–81. [PubMed: 12876221]
24. Tzima E, del Pozo MA, Shattil SJ, Chien S, Schwartz MA. Activation of integrins in endothelial cells by fluid shear stress mediates Rho-dependent cytoskeletal alignment. EMBO J 2001;20:4639–47. [PubMed: 11532928]
25. Kim M-H, Harris NR, Tarbell JM. Regulation of capillary hydraulic conductivity in response to an acute change in shear. Am J Physiol Heart Circ Physiol 2005;289:H2126–H35. [PubMed: 15994851]
26. Williams DA. Change in shear stress ($\Delta\tau$)/hydraulic conductivity (L_p) relationship after pronase treatment of individual capillaries *in situ*. Microvasc Res 2007;73:48–57. [PubMed: 17030043]
27. Jo H, Dull RO, Hollis TM, Tarbell JM. Endothelial albumin permeability is shear dependent, time dependent, and reversible. Am J Physiol 1991;260:H1992–H6. [PubMed: 1905493]
28. Colgan OC, Ferguson G, Collins NT, Murphy RP, Meade G, Cahill PA, et al. Regulation of bovine brain microvascular endothelial tight junction assembly and barrier function by laminar shear stress. Am J Physiol Heart Circ Physiol 2007;292:H3190–H7. [PubMed: 17308001]
29. DeMaio L, Tarbell JM, Scaduto RC Jr, Gardner TW, Antonetti DA. A transmural pressure gradient induces mechanical and biological adaptive responses in endothelial cells. Am J Physiol Heart Circ Physiol 2004;286:H731–H41. [PubMed: 14527936]
30. Kim M-H, Harris NR, Tarbell JM. Regulation of hydraulic conductivity in response to sustained changes in pressure. Am J Physiol Heart Circ Physiol 2005;289:H2551–H8. [PubMed: 16113077]
31. Suttorp N, Hessz T, Seeger W, Wilke A, Koob R, Lutz F, et al. Bacterial exotoxins and endothelial permeability for water and albumin in vitro. Am J Physiol 1988;255:C368–C76. [PubMed: 3138913]
32. Wong KHK, Truslow JG, Tien J. The role of cyclic AMP in normalizing the function of engineered human blood microvessels in microfluidic collagen gels. Biomaterials. in press.
33. Price GM, Chrobak KM, Tien J. Effect of cyclic AMP on barrier function of human lymphatic microvascular tubes. Microvasc Res 2008;76:46–51. [PubMed: 18440562]
34. Rubin LL, Hall DE, Porter S, Barbu K, Cannon C, Horner HC, et al. A cell culture model of the blood-brain barrier. J Cell Biol 1991;115:1725–35. [PubMed: 1661734]

35. Huxley VH, Curry FE, Adamson RH. Quantitative fluorescence microscopy on single capillaries: α-lactalbumin transport. Am J Physiol 1987;252:H188–H97. [PubMed: 3492924]
36. Price, GM.; Tien, J. Methods for forming human microvascular tubes in vitro and measuring their macromolecular permeability. In: Khademhosseini, A.; Suh, K-Y.; Zourob, M., editors. Biological Microarrays (Methods in Molecular Biology series). Totowa, NJ: Humana Press; in press
37. Truslow JG, Price GM, Tien J. Computational design of drainage systems for vascularized scaffolds. Biomaterials 2009;30:4435–43. [PubMed: 19481796]
38. Corada M, Mariotti M, Thurston G, Smith K, Kunkel R, Brockhaus M, et al. Vascular endothelial-cadherin is an important determinant of microvascular integrity *in vivo*. Proc Natl Acad Sci USA 1999;96:9815–20. [PubMed: 10449777]
39. Heupel W-M, Efthymiadis A, Schlegel N, Muller T, Baumer Y, Baumgartner W, et al. Endothelial barrier stabilization by a cyclic tandem peptide targeting VE-cadherin transinteraction in vitro and in vivo. J Cell Sci 2009;122:1616–25. [PubMed: 19420236]
40. Fu BM, Shen S. Acute VEGF effect on solute permeability of mammalian microvessels in vivo. Microvasc Res 2004;68:51–62. [PubMed: 15219420]
41. Nichol J, Girling F, Jerrard W, Claxton EB, Burton AC. Fundamental instability of the small blood vessels and critical closing pressures in vascular beds. Am J Physiol 1951;164:330–44. [PubMed: 14810938]
42. Tzima E, Del Pozo MA, Kiosses WB, Mohamed SA, Li S, Chien S, et al. Activation of Rac1 by shear stress in endothelial cells mediates both cytoskeletal reorganization and effects on gene expression. EMBO J 2002;21:6791–800. [PubMed: 12486000]
43. Waschke J, Drenckhahn D, Adamson RH, Barth H, Curry FE. cAMP protects endothelial barrier functions by preventing Rac-1 inhibition. Am J Physiol Heart Circ Physiol 2004;287:H2427–H33. [PubMed: 15271660]
44. Potter DR, Damiano ER. The hydrodynamically relevant endothelial cell glycocalyx observed in vivo is absent in vitro. Circ Res 2008;102:770–6. [PubMed: 18258858]
45. Hecker M, Mulsch A, Bassenge E, Busse R. Vasoconstriction and increased flow: two principal mechanisms of shear stress-dependent endothelial autacoid release. Am J Physiol 1993;265:H828–H33. [PubMed: 8105699]
46. Ueda A, Koga M, Ikeda M, Kudo S, Tanishita K. Effect of shear stress on microvessel network formation of endothelial cells with in vitro three-dimensional model. Am J Physiol Heart Circ Physiol 2004;287:H994–H1002. [PubMed: 15130887]
47. Kang H, Bayless KJ, Kaunas R. Fluid shear stress modulates endothelial cell invasion into three-dimensional collagen matrices. Am J Physiol Heart Circ Physiol 2008;295:H2087–H97. [PubMed: 18805898]
48. Zamir M. Optimality principles in arterial branching. J Theor Biol 1976;62:227–51. [PubMed: 994521]

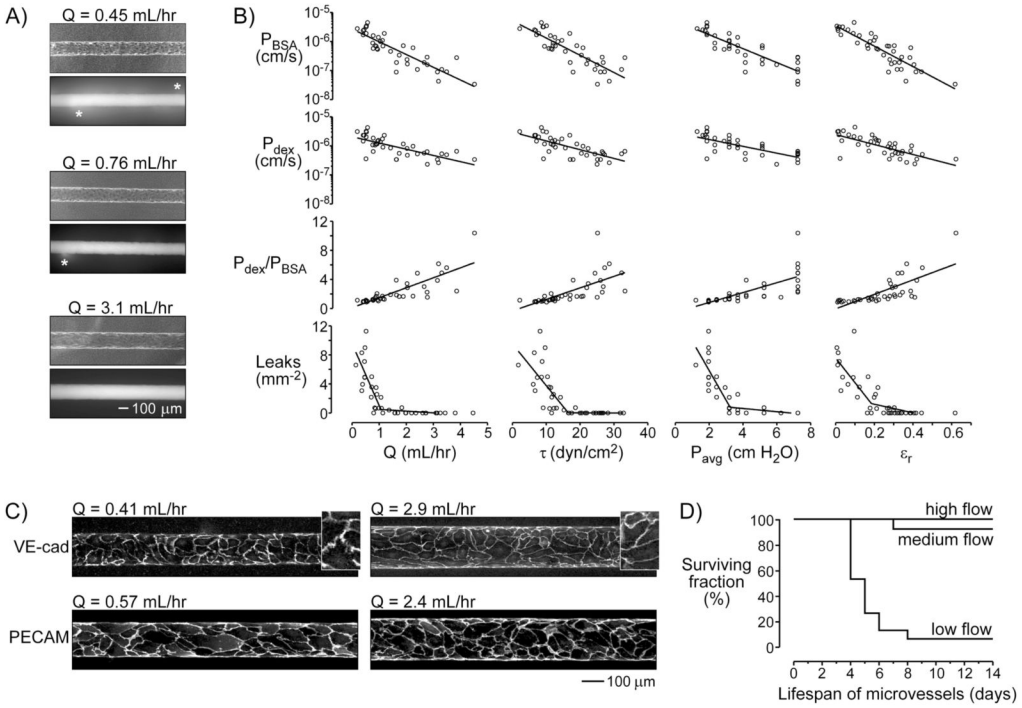

Figure 1.

Effect of flow on the barrier function and stability of engineered microvessels. (A) Phase-contrast images of microvessels maintained under different flow conditions, and fluorescence images after perfusion with Alexa Fluor 594-conjugated bovine serum albumin (BSA). Asterisks denote focal leaks. (B) Plots of permeability coefficients to BSA and dextran (P_{BSA} and P_{dex}), size selectivity (P_{dex}/P_{BSA}), and focal leak density versus flow rate (Q), shear stress (τ), average lumenal pressure (P_{avg}), and radial strain (ε_r). All trends were significant ($p < 0.0001$). Lines denote linear fits for permeabilities and selectivities, and piecewise fits for focal leak densities. (C) Immunostaining of VE-cadherin (VE-cad) and PECAM. *Insets*, VE-cadherin staining magnified 2.3×. (D) Kaplan-Meier plots under low, medium, and high flows. Low flow decreased vascular lifespan significantly ($p < 0.0001$).

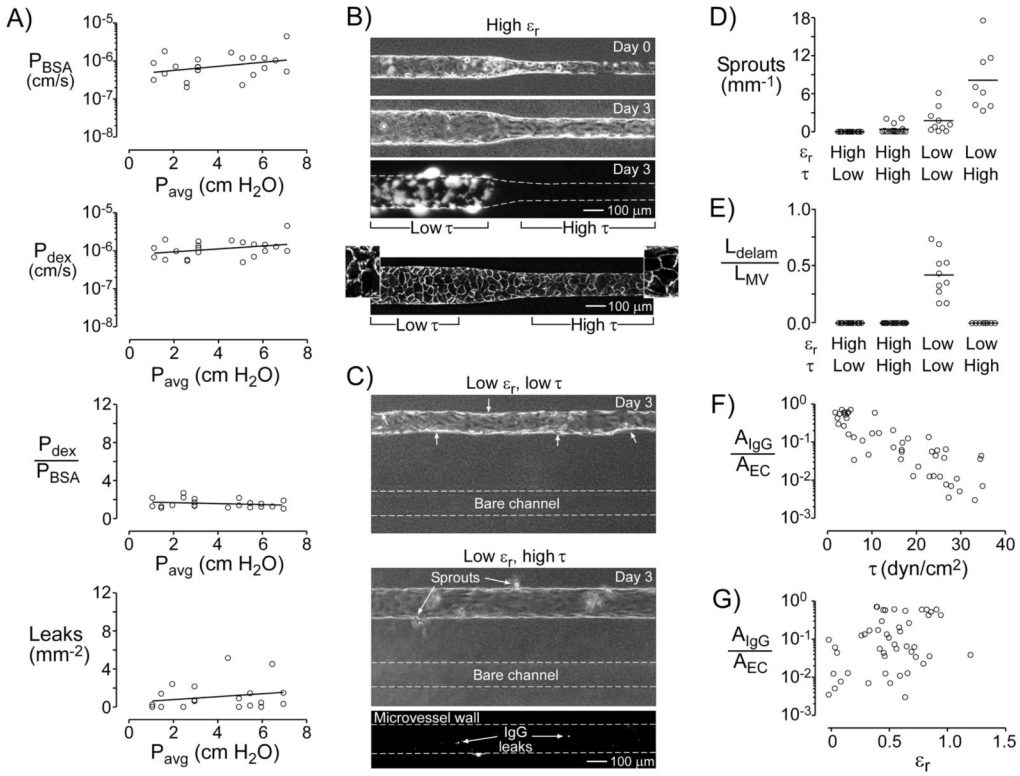

Figure 2.

Effects of lumenal pressure (P_{avg}), shear stress (τ), and strain (ε_r) on the barrier function and stability of engineered microvessels. (A) Plots of permeability coefficients, size selectivity, and focal leak density of vessels in which average lumenal pressure was selectively varied. Linear regression of the data (black lines) did not significantly differ from a slope of zero ($p > 0.1$). (B–C) Phase-contrast and fluorescence images of engineered microvessels at day 0 (day of seeding) and/or at day 3. Fluorescent signal indicates positive staining by antibodies to collagen. Direction of flow is from left to right. (B) Vessels with a tapered geometry had high strain and variable shear stress. *Third panel*, fluorescence image after labeling leaks with antibody to collagen. *Bottom panel*, fluorescence image of VE-cadherin expression. *Insets*, VE-cadherin staining magnified 2.3×. (C) Vessels in parallel with bare channels had low strain and variable shear stress. *Top panel*, vessel maintained under low shear. Small arrows indicate regions of delamination. *Middle panel*, vessel maintained under high shear. *Bottom panel*, fluorescence image after labeling leaks. (D) Plot of sprouting, defined as number of sprouts per length of microvessel, under various shears and strains. (E) Plot of delamination, defined as the total length of delamination per length of microvessel (L_{delam}/L_{MV}), under various shears and strains. (F–G) Plots of normalized leak area (A_{IgG}/A_{EC}) versus shear or strain. For the effect of shear stress, $p < 0.0001$. For the effect of strain, $p > 0.05$.

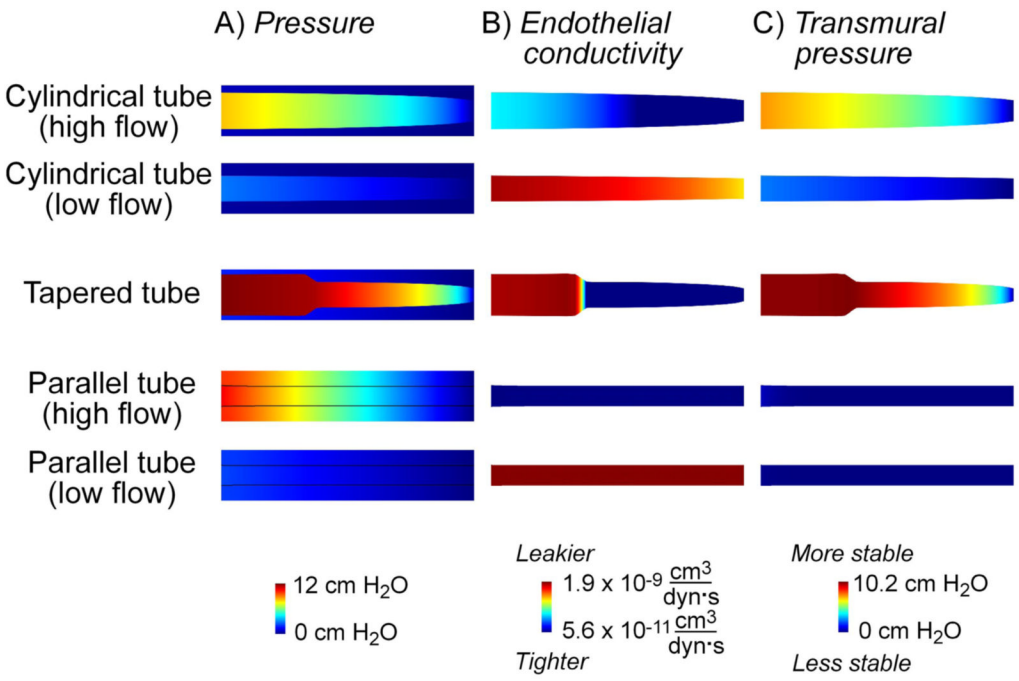

Figure 3.

Prediction of vascular phenotype with computational models. Flow is from left to right. Images are shown for a ratio of permeability coefficient to BSA and endothelial hydraulic conductivity of 1000 dyn/cm^2; ratios of 500 and 2000 dyn/cm^2 produced similar results. For ease of visualization, only the regions within 150 μm of vessel centerlines are shown; bare channels are not shown. Cylindrical and tapered tubes are 9-mm-long, and parallel tubes are 9.5-mm-long; vascular profiles with calculated radial strains are shown. (A) Maps of lumenal and gel pressures. (B) Maps of endothelial hydraulic conductivity, using the solved shear stress and extrapolation from the linear fit in Figure 1B. (C) Maps of transmural pressure.

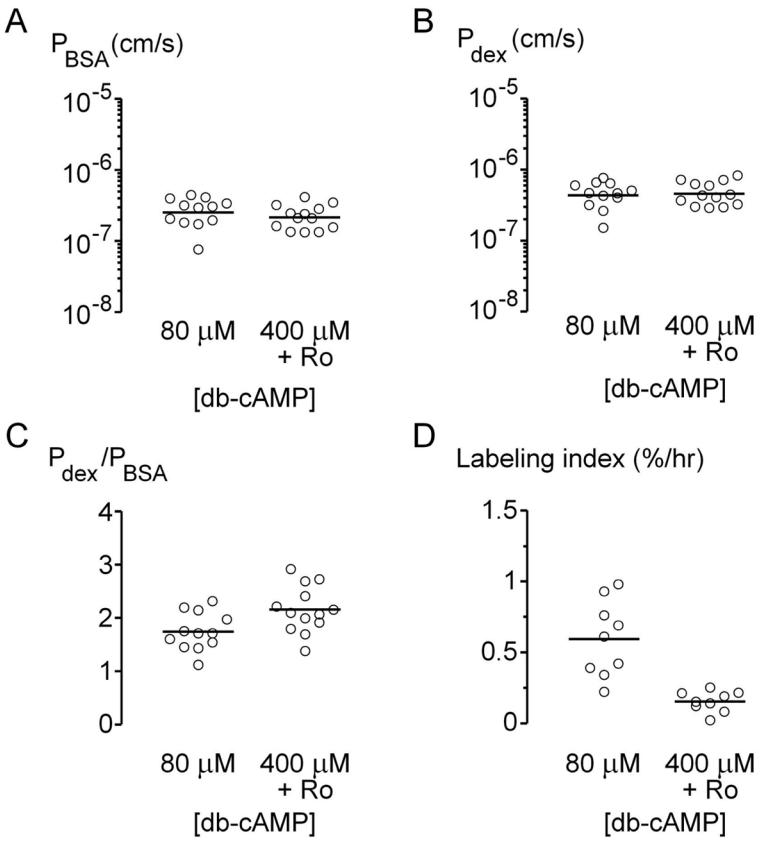

Figure 4.

Effect of elevated cAMP levels on barrier function (A–C) and proliferation rates (D) in microvessels under high flow. Increasing amounts of cAMP led to higher selectivity ($p = 0.03$) and lower proliferation rates ($p < 0.0001$).